



An experimental study on flow patterns and heat transfer characteristics during cryogenic chilldown in a vertical pipe

Hong Hu^{a,*}, Jacob N. Chung^a, Samuel H. Amber^b

^a Department of Mechanical and Aerospace Engineering, University of Florida, Gainesville, Florida 32611, United States

^b Department of Physics and Nuclear Engineering, U.S. Military Academy, West point, New York 10928, United States

ARTICLE INFO

Article history:

Available online 6 March 2012

Keywords:

Cryogenics
Quenching
Flow boiling
Heat transfer

ABSTRACT

In the present paper, the experimental results of a cryogenic chilldown process are reported. The physical phenomena involve unsteady two-phase vapor–liquid flow and intense boiling heat transfer of the cryogenic fluid that is coupled with the transient heat conduction inside pipe walls. The objective for the present study is to compare the chilldown rates and flow patterns between the upward flow and downward flow in a vertical pipe. Liquid nitrogen is employed as the working fluid and the test section is a vertical straight segment of a Pyrex glass pipe with an inner diameter of 8 mm. The effects of mass flow rate on the flow patterns, heat transfer characteristics and interface movement were determined through experiments performed under several different mass flow rates. Through flow visualization, measurement and analysis on the flow patterns and temperature variations, a physical explanation of the vertical chilldown is given. By observing the process and analyzing the results, it is concluded that pipe chilldown in a vertical flow is similar to that in microgravity to some extent.

© 2012 Elsevier Ltd. All rights reserved.

1. Introduction

Cryogenic fluids are involved in the propulsion and thermal management for space missions, medical applications and industrial processes. According to the U.S. Space Launch System (SLS), for the Multi-Purpose Crew Vehicle (MPCV) [1], liquid hydrogen (LH₂) and liquid oxygen (LOX) are used as the fuel for RS-25 and J-2X rocket engines. On the other hand, liquid nitrogen (LN₂) and liquid helium (LHe) are usually employed as coolants for satellites and superconductors such as those in commercial MRI, NMRI, MRT and the Large Hadron Collider (LHC) [2,3]. In many of these applications the cryogenic fluids are initially introduced into piping systems whose temperatures are much higher than the saturation temperature of the working fluids. An intense evaporation of the cryogen is expected to occur in the pipe. It is an ineluctable stage before the cryogenic fluid can be transferred in a liquid state, known as the pipe chilldown. The complexity of the chilldown process is a result of the intricate interaction between the two-phase flow and the boiling heat transfer. With respect to particular physical properties (e.g., small surface tensions, small latent heats, near zero wetting angles and large ratios of vapor density to liquid density), most of the current empirical and semi-empirical correlations, and research findings for heat and mass transfer would break down

under cryogenic conditions. Moreover, most of the space systems are structured in a vertical position on the ground at the initial stage, such as the pipes connecting the propellant to the oxidant storage chamber and combustion chamber inside the rocket during the launch. Therefore it is necessary to study the vertical pipe chilldown process under terrestrial conditions. The current research aims to offer some physical understandings regarding the chilldown phenomena and provide reliable tools for the design of a cryogenics system.

1.1. Flow regimes during pipe chilldown

There has been a large amount of studies on the flow regimes during boiling of normal fluids such as water, FC-72 and R-113. Manera et al. [4], have studied the flow pattern transition in an upward flashing flow with wire-mesh sensors and provided a time-depend special distribution of steam/water inside the pipe. Estrada-Perez et al. [5] used time resolved particle tracking velocimetry (PTV) to investigate a turbulent, subcooled boiling flow of refrigerant HFE-301 through a vertical rectangular channel.

With respect to special physical properties and a wide application of cryogenics, the flow boiling heat transfer and flow pattern development on cryogenic transport have received increasing attention in recent years. Zhang and Fu [6] investigated the flow patterns through experimental research on vertical and upward flows in 0.5 and 1.0 mm micro tubes. Furthermore, a 3-D visualization

* Corresponding author. Tel.: +1 3522154588.

E-mail address: hydrogen@ufl.edu (H. Hu).

Nomenclature

q''	heat flux (W/m ²)	μ	viscosity (Ns/m ²)
G	mass flow rate (kg/m ² s)	σ_B	Stefan Boltzmann constant
T	temperature (K)	δ	chamber inner spacing (m)
h	heat transfer coefficient (W/m ² K)	ε	emissivity
k	thermal conductivity (W/K)		
d	tube diameter (mm)	<i>Subscripts</i>	
P	pressure (kPa)	c	chilldown
h_{fg}	latent heat (kJ/kg)	o	outer wall
C	specific heat (J/kg K)	l	liquid
r	tube radius (mm)	sat	saturated condition
t	time (s)	i	inner wall
g	gravitational acceleration constant	sub	subcooling
Nu	Nusselt number	w	tube wall
Ra	Rayleigh number	v	vapor
Pr	Prandtl number	rew	rewetting
L	test section length (m)	ch	vacuum chamber
		$conv$	convection heat transfer
<i>Greek symbols</i>		rad	radiation heat transfer
α	thermal diffusivity (m ² /s)	$cond$	conduction heat transfer
ρ	density (kg/m ³)	$quen$	quench front
σ	surface tension (mN/m)	CHF	critical heat flux
β	thermal expansion coefficient (K ⁻¹)		

technique [7] has been developed to analyze the bubble dynamics and flow pattern evolution with a higher accuracy. Fu et al. [8] revealed detailed physical explanations on cryogenic bubble dynamics inside the vertical pipe.

Although there is a substantial amount of data available for cryogenic boiling, none of them can be used to solve quench problem directly due to the difference in flow patterns between boiling and quenching. It is believed that the transition boiling regime and the switch-over between nucleate boiling and natural convection contribute most to the complexity of the problem.

Subcooled water has been used as the working fluid for the chilldown experiment by Barnea et al. [9]. They have studied the quenching front movement and the volumetric void fraction as a function of the distance from the quench front. A unique flow pattern, the filament flow, which has been found in microgravity condition by Antar et al. [10], was observed even in a terrestrial condition experiment by Kawanami et al. [11]. This flow pattern appeared only in the downward flow, large tube diameter and high mass velocity conditions. They also pointed out that the gravity effects on heat transfer of forced convective boiling decrease with an increase in the mass velocity.

1.2. Effects of gravity and flow direction on chilldown

Pipe chilldown is affected not only by the mass flow rate, initial wall superheat, and liquid subcooling, but also by the gravity and orientation of the tube that bring large effects to the flow pattern development and corresponding heat transfer characteristics. Microgravity experiments with both horizontal and vertical pipes have been performed on parabolic flights and in a drop tower worldwide in the past several decades. Quenching of a horizontal hot stainless steel tube by injecting R-113 was investigated by Westbye et al. [12] under both terrestrial gravity and microgravity conditions. The conclusion achieved is that heat transfer coefficients in microgravity were only 20–50% of those obtained in normal gravity and the rewetting temperatures were also found to be 15–20 K lower in microgravity.

Comparing to the horizontal flow, it is believed that chilldown in a vertical pipe is less affected by gravity and it is easier to capture the movement of the quenching front than in the horizontal pipe. Verthier et al. [13] carried out several vertical quenching experiments using FC-72 and pointed out that the flow pattern in microgravity was closer to that in an upward flow due to the rising of vapor bubbles. Also more experiments on FC-72 were conducted by Celata et al. [14] during parabolic flight microgravity experiments. They stated that the mass flow-rate had a significant influence on the flow structure and the behavior of the liquid core during the inverted annular flow regime.

Because of the difficulties in the design of the experiment and in conducting the work, there are fewer chilldown data for cryogenic fluids compared to normal fluids. Liquid nitrogen was used as the working fluid in tests of Kawanami et al. [15] to investigate the heat transfer characteristics and flow pattern during the quenching of a vertical tube. The tests were conducted under both terrestrial condition and a ten-second microgravity condition with the help of the drop tower in the Japan Microgravity Center (JAMIC). They claimed that the heat transfer and quenching front velocity under microgravity condition increased up to 20% compared to those in the normal gravity condition.

Furthermore, Yuan et al. [16] have conducted a series of experiments on LN2 chilldown in a horizontal pipe in both terrestrial condition and the microgravity environment created by a 1.8 s drop tower. According to their results the liquid droplets tended to form filaments and settled down on the bottom of the test section in the terrestrial gravity condition with decreasing temperature. At this time, the separation of vapor and liquid led to the different heat transfer mechanism at the top and bottom of the pipe, respectively due to gravity. While in the drop tower test, a lower heat transfer efficiency was observed due to a stable and thick vapor film surrounding the liquid core.

With the goal of improving the knowledge of the chilldown process in pipes, the present paper mainly focused on the heat transfer characteristics in the vertical tube experiments under the terrestrial condition. The effects of the gravity and flow orientation were analyzed though a comparison between the results of upward and downward flow experiments.

Table 1
Principal physical properties of LOX and LN2 [17].

Parameters	LOX	LN2
ρ_l (kg/m ³)	1135.72	807.10
T_{sat} (K)	90.18	77.35
h_{fg} (kJ/kg)	212.3	197.6

2. Experiment

2.1. Experimental apparatus

LN2 was selected as the test fluid in the present study not only for the safety consideration but also because its surface tension, boiling point and evaporative latent heat are similar to those of liquid oxygen, as shown in Table 1. The initial temperature of the test section was kept at the normal room temperature (around 293 K).

The highly integrated test apparatus, as shown in Fig. 1, was composed of a pressurized liquid nitrogen tank (Airgas 180Lts 22PSI), a stainless steel tube casing (MDC), thermocouples (Omega) and a DAQ (Measurement Computing PCI-DAS-TC), a mass flow rate meter (Sensirion EM1), a vacuum pump (HyVac PressoVac 24) and a high speed camera (Redlake MotionScope PCI 8000s). The apparatus frame was constructed from 1" × 1" extruded aluminum 80/20 made from 6105-T5 aluminum alloy, a widely used industrial erector set.

A schematic of system is shown in Fig 2. The LN2 was driven to flow through a main adjusting valve into a transparent pipe housed inside a stainless steel chamber which provided a vacuum environment to insulate the tube. The valve controlled the mass flow rate into the test section. When the mass flow rate was larger than the preset-value, the liquid would flow into the bypass pipe and finally vented into the atmosphere.

Two glass ports (Fig. 1) in the vacuum chamber are used for the high speed camera and background lighting. The high speed camera caught the video of flow pattern development. After that, the two-phase flow entered a heat exchanger, where the two-phase flow fully evaporated into a pure nitrogen gas. Finally a mass flow rate meter measured the gas flow rate before it is vented into the atmosphere.

The thermocouples were used to acquire the transient temperature data along the tube. A total of 15 thermocouples were glued on the outer surface of the tube at five different sections with a separating distance of 20 mm, as Fig. 3 shows. At each location, three thermocouples were located circumferentially at equal separation

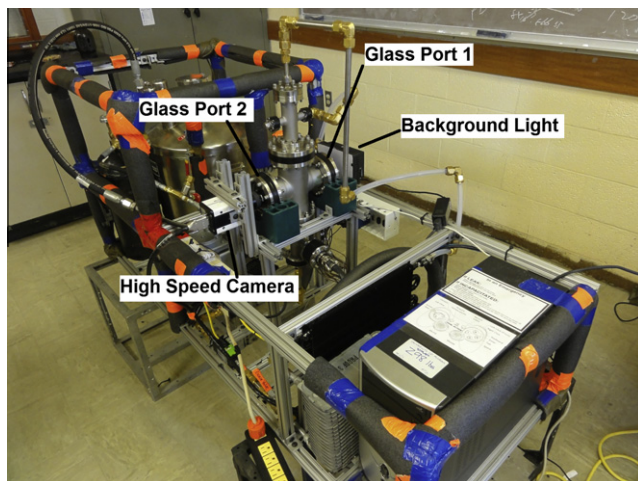


Fig. 1. Overview of test apparatus.

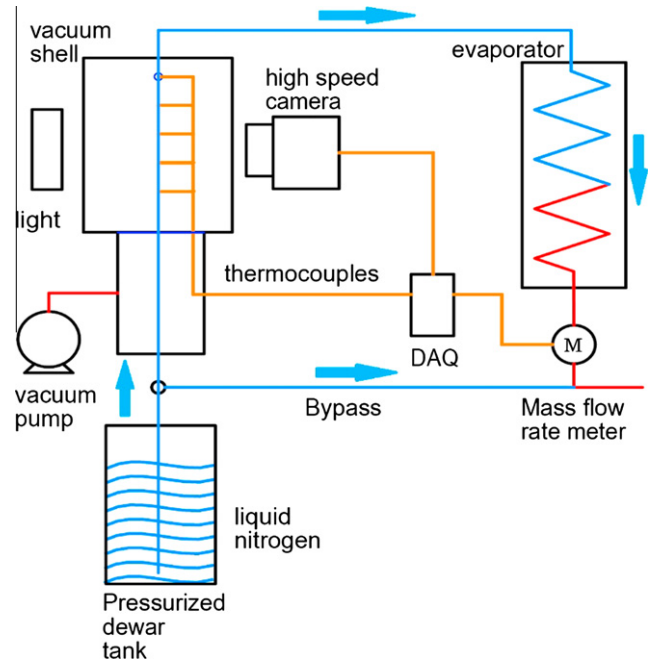


Fig. 2. Schematic of system set-up.

distance. These were type *T* thermocouples (Omega) with Teflon insulation and the gauge size of the thermocouple wires was 30 AWG. A specialized cryogenic epoxy resin, LakeShore Low Temperature Conductive Epoxy which had a very limited volume resistivity at the range of 0.0001–0.0004 W cm, was used. After it was cured, the epoxy turned into complete solid, which was less than 2 mm in height. Therefore, the time delay of the temperature measurement due to the epoxy could be neglected.

3. Uncertainty analyses

In the current experiment, the inverse heat conduction problem introduced by Ozisik et al. [18,19] needed to be solved in order to obtain the surface heat flux from the temperatures measured. Both the uncertainties from the experimental apparatus and from the parameters derived from equations have been listed in Table 2. The uncertainties mainly came from measurements from thermocouples, DAQ, mass flow rate meter and vacuum leakage from the chamber.

The type *T* thermocouples used for the temperature measurement had the uncertainty of ± 0.50 K suggested by the manufacturer. Another uncertainty source for temperature measurement comes from the data acquisition (DAQ) system. It was found that the uncertainty was ± 0.30 K when the gain was set at 400, the sampling rate was 60 Hz and type *T* thermocouples were used, according to the data sheet. Another measurement uncertainty was caused by the mass flow rate meter. The integrated temperature sensor inside the meter automatically provided a real-time revision on the mass flow rate due to temperature fluctuations. When the flow range was set between 0 and 200 L/min, the sensor returned a value with $\pm 5\%$ accuracy and 0.5% repeatability of full scale of measured value. For the current experiment, the vacuum level inside the chamber was measured by a vacuum gauge that had the uncertainty of 0.01 bar.

4. Result and discussion

The test was carried out with reference to thermal hydraulic conditions as reported in Table 3. In this section, a series of detailed

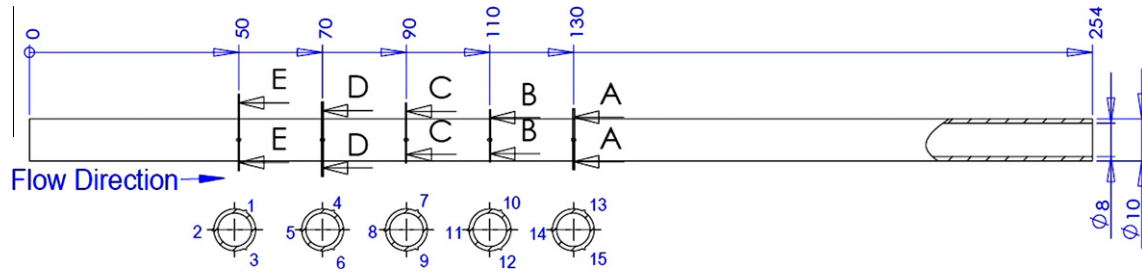


Fig. 3. Locations of thermocouples.

Table 2
Summary of the uncertainty.

Parameter measured	Uncertainty
D (mm)	0.001
T_o (K0029)	0.8
G (%)	5
Vacuum level (bar)	0.01
Parameter derived	Uncertainty
T_i (K)	0.8
q_i (%)	6.8
h_i (%)	6.8

Table 3
The range of the main experimental parameters.

d_i (mm)	8.00
d_o (mm)	10.00
d_{ch} (mm)	145.8
G (kg/m ² s)	20–80
T_{sub} (K)	0
T_w (K)	293
Flow directions	Upward and downward
P_o (kPa)	101.3

analyses will be presented on heat transfer characteristics, flow pattern development and quenching front movement.

4.1. Heat transfer characteristic

Heat transfer characteristic analysis is the most important part of the research. Based on the comparison among the temperature profile, heat flux, heat transfer coefficient and critical heat flux (CHF) under various mass flow rates and flow directions, some physical explanations are revealed. Temperature profile indicates

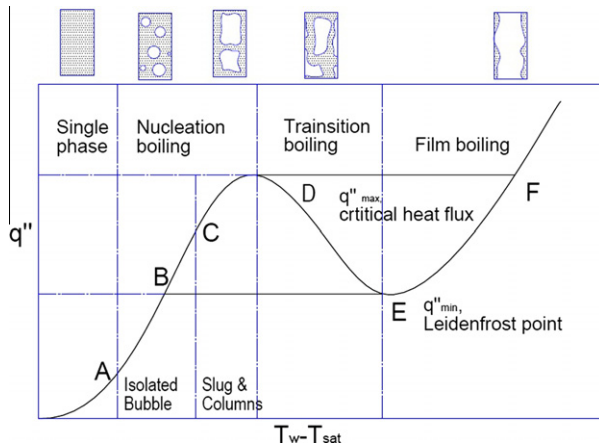


Fig. 4. Typical boiling curve and flow patterns.

an intuitive view on how LN2 quenches the tube walls and how fast the tube is cooled down. The analysis on heat flux and temperature will help to determine the heat transfer mechanisms during the chilldown process and serves for the comparison between chilldown of different orientations.

Before carefully studying the chilldown process, a brief review on boiling process is necessary. A typical saturated boiling curve plotted in Fig. 4 shows the relationship between the heat flux and the wall temperature. A cryogenic chilldown process usually starts from point F and then goes towards point E in the film boiling regime as the wall temperature decreases. Point E is usually called the Leidenfrost point which signifies the minimum wall temperature required for the film boiling. When cooling beyond the Leidenfrost point, the boiling process will proceed from E to D in the transition boiling regime, which is characterized by a decreasing of wall temperature with an increasing heat flux. Quench front will be observed at point D, where the CHF occurs. After passing it, the heat transfer mechanism then changes to nucleate boiling with decreases both in the heat flux and temperature.

In order to study the heat transfer characteristics quantitatively, the inner wall temperature and heat flux need to be known. The inner wall temperature profile can be derived from the temperatures acquired from the thermocouples glued on the outer surface of the pipe. Burggraf [20] developed a method to obtain the temperatures and heat fluxes at the inside tube wall from the temperature history data of the thermocouple welded on the outside of the test section as follows:

$$T_i = T_o + \left(\frac{r_o^2}{4\alpha} \left(\left(\frac{r_i}{r_o} \right)^2 - 1 - 2 \ln \left(\frac{r_i}{r_o} \right) \right) \right) \frac{dT_o}{dt} + \left(\frac{1}{64\alpha^2} (r_i^5 - 5r_o^4) - \frac{r_o^2 r_i^2}{8\alpha^2} \ln \left(\frac{r_i}{r_o} \right) - \frac{r_o^4}{16\alpha^2} \ln \left(\frac{r_i}{r_o} + \frac{r_o^2 r_i^2}{16\alpha^2} \right) \right) \frac{d^2 T_o}{dt^2} + \dots \quad (4.1)$$

This method has been used by Yuan et al. [16] to acquire the inner wall temperature. The temperature profiles measured from the embedded thermocouples at two among the five different cross-sections with different mass fluxes are shown in Figs. 5 to evaluate the inner wall temperature changes.

It is clear that the temperature profile can be divided into three distinct phases for both upward and downward flows. The first phase covers approximately the first twenty seconds where the wall temperature is relatively flat. During this short initial period, the fluid evaporated completely inside the connection pipes before entering the test section. The test section is filled entirely by vapor that does not have much contribution to lower the wall temperature. The second phase then begins as the vapor is convected downstream that allows the fresh liquid to take its place, but the wall is still hot so a vapor film would cover the wall with small liquid droplets flowing in the core to form a dispersed droplet flow with film boiling heat transfer taking place. So during the second phase, the wall starts to get cooled down at a relatively constant rate. It is obvious that the second phase lasts longer in the upward flow and the quench front arrives in the downward flow much faster than the upward flow. The third phase is distinguished from the second

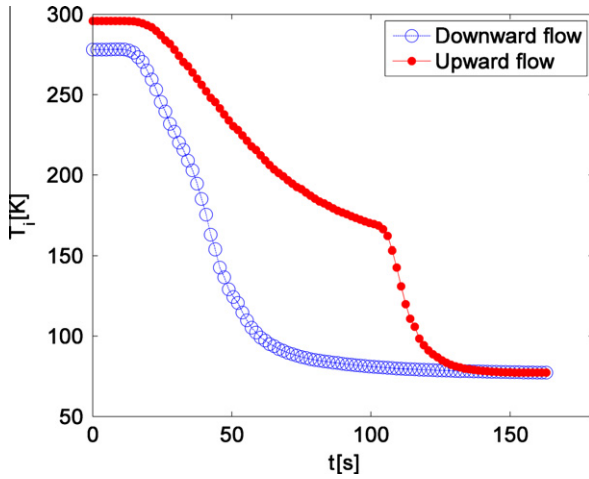


Fig. 5. Comparison between upward and downward flows for $G = 66 \text{ kg/m}^2 \text{ s}$.

phase by a different cooling slope and it starts around 115 s and 60 s (Fig. 5) for upward and downward flows, respectively. Similar to the data by Westbye et al. [12], the downward flow chilldown is similar to that in a normal gravity horizontal pipe, while the chilldown curve for the upward flow is closer to that in a microgravity condition. Therefore it is reasonable to use the upward flow to simulate the microgravity flow to some extent. The transition from Phase 2 to 3 corresponds to the so-called Leidenfrost point, it happens when the wall is cooled down to a low enough temperature to allow the liquid first to wet the wall directly. During the third phase in the nucleation boiling regime, the heat transfer coefficients are larger and results in a faster cooling rate.

It is difficult to distinguish between the transition boiling and nucleation boiling regimes only from the temperature profile. As compared to the temperature profile, the heat flux profile can reveal more information regarding the heat transfer regimes, flow pattern development and other phenomena. In order to estimate the heat flux at the inner wall, an energy balance question is needed. This method has been used by several researchers [12,16]. For a vertical chilldown experiment, the radial heat conduction can be neglected because that the axisymmetric assumption can be reasonably employed. Therefore the energy equation [16] for the inner wall of the tube can be simplified as:

$$q_i'' = q_{cond}'' + q_{quench}'' - \frac{r_o}{r_i} (q_{conv}'' + q_{rad}'') \quad (4.2)$$

The second term is the axial heat conduction. It is a normal practice to neglect this term [15] because this term has been proved to be very small except at the quench front, where there is a large temperature gradient between the wet surface and dry surface. The first term in Eq. (4.2) is the heat conduction of the inner wall, which can be acquired by the first three leading terms in the Fourier series derived from the temperature profile [16]:

$$q_{cond}'' = \rho C \left(\frac{r_i^2 - r_0^2}{2r_i} \right) \frac{dT_o}{dt} + \left(\frac{\rho C}{k} \left(\frac{r_i^3}{16} - \frac{r_0^4}{16r_i} - \frac{r_0^2 r_i}{4} \ln \left(\frac{r_i}{r_0} \right) \right) \right) \frac{d^2 T_o}{dt^2} + \frac{(\rho C)^3}{k^2} \left(\frac{r_i^5}{384} - \frac{3r_0^4 r_i}{128} + \frac{3r_0^2 r_i^3}{128} - \frac{r_0^6}{384r_i} - \frac{r_0^2 r_i^3}{32} \ln \left(\frac{r_i}{r_0} \right) - \frac{r_0^4 r_i}{32} \ln \left(\frac{r_i}{r_0} \right) \right) \frac{d^3 T_o}{dt^3} \quad (4.3)$$

The third term in Eq. (4.2) represents the natural convection inside the vacuum chamber due to the residual air. It can be reasonably assumed to be the natural convection in an annular space between concentric vertical cylinders. The vertical annular space is

axisymmetric, which can reduce the problem from three-dimensional to two-dimensional. The average Nu number and heat transfer coefficient can be calculated with the aid of a rectangle enclosure correlation as the following:

$$Nu_L = \frac{\bar{h}\delta}{k} = 0.22 \left(\frac{\text{Pr}Ra_\delta}{0.2 + \text{Pr}} \right)^{0.28} \left(\frac{L}{\delta} \right)^{-0.25} \quad (4.4)$$

$$Ra_\delta = \frac{\beta g (T_{ch} - T_o) \delta^3 \rho^2}{\mu^2} \text{Pr} \quad (4.5)$$

$$\delta = \frac{1}{2} (d_{ch} - d_i) \quad (4.6)$$

$$q_{conv}'' = \pi d_o \bar{h} (T_{ch} - T_o) \quad (4.7)$$

Apart from the convection, the contribution of radiation, the fourth term in Eq. (4.2), also needs to be considered. Assuming the vacuum chamber and the test section constitute to a long concentric cylinder, the radiation can be calculated as the following:

$$q_{rad}'' = \frac{\sigma_B}{\frac{1}{\epsilon_i} + \frac{1 - \epsilon_{ch}}{\epsilon_{ch}} \left(\frac{d_o}{d_{ch}} \right)} (T_{ch}^4 - T_o^4) \quad (4.8)$$

Therefore, we can calculate the inner wall heat flux from the temperature profile measured by the thermocouples by putting these equations together.

Regarding to the heat flux profiles, shown in Fig. 6, two peaks are found in each of the two graphs. The first one on the right represents the maximum heat flux for film boiling, which appears at the beginning of the chilldown. The one on the left is the critical heat flux (CHF) which is the highest heat flux during chilldown. From Fig. 6, it is clear that the overall heat flux for the downward flow is higher than that for the upward flow, which answers the question that why the total chilldown time for the downward flow is much less. In spite of the difference on the magnitudes, the heat flux profiles for both directions are of the same shapes and on the same order of magnitude, which means there is no difference in the heat transfer mechanisms. Although the heat flux has a greater uncertainty as compared to the temperature, the heat flux profiles for the nucleate boiling regime obtained for the upward and downward flows are similar, which shows that this regime is probably less affected by the orientation. Thus, the temperature and heat flux profiles can be put together to provide a complete understanding on the overall heat transfer characteristics.

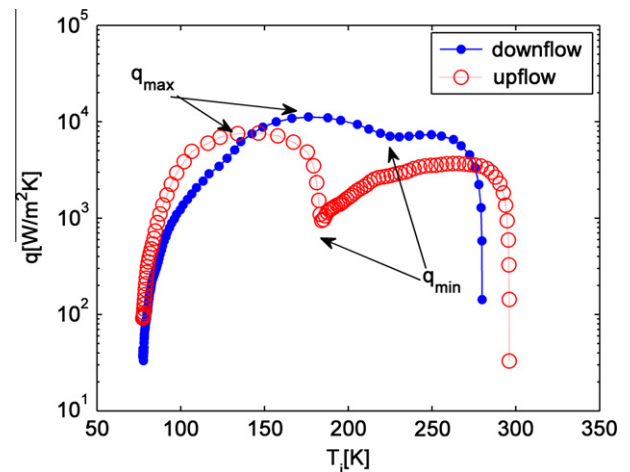


Fig. 6. Comparison of heat fluxes between the upward and downward flows for $G = 66 \text{ kg/m}^2 \text{ s}$.

In Fig. 7, the shape of the heat flux is similar to the boiling curve from the steady state pool boiling experiment. q_{min} and q_{max} are used to divide the different regimes of boiling that are film boiling, transition boiling and nucleation boiling. Film boiling will be the main heat transfer mechanism at the initial stage due to the large temperature differences between the wall and the inlet liquid. The heat flux decreases linearly due to the nearly constant heat transfer coefficient and decreasing wall superheat. Transition boiling follows when the Leidenfrost temperature is reached. The unique heat transfer characteristics of decreasing wall superheat with increasing heat flux leads to the unstable heat transfer. The transition boiling has large effects on the following boiling regimes. Soon after it, the CHF appears to be the highest heat flux and a sign of the transition to nucleation boiling where a rapid phase change is involved. After the heat flux is calculated, the heat transfer coefficient h_w at the inner wall of the tube is given by

$$q_i'' = -k \frac{\partial T}{\partial r} \tag{4.9}$$

$$h_i = \frac{q_i''}{T_i - T_{sat}} \tag{4.10}$$

Regarding to the heat transfer coefficient profiles in Figs. 8, it is clear that the film boiling continues for longer time and the heat transfer coefficient is more stable under the upward flow condition. Also, from the figures, it is clear that nucleation boiling heat transfer coefficient is almost one order of magnitude higher than that of the film boiling.

The direction of the flow not only has an influence on the total time for chilldown, but the heat flux profile, critical heat flux and the heat transfer coefficient are all affected. In order to clarify this effect, a comparison between the upward and downward flow on the chilldown time, heat flux profile and CHF will be discussed later.

As Fig. 9 shows, almost 30% to 40% longer chilldown time is needed for the upward flow with the same mass flow rate. A linear function is used to best fit the data. It is also obvious that with the increase of the liquid mass flow rate, the difference in chilldown time is reduced. The well-known Zuber's model for saturated pool boiling is given:

$$q'' = 0.131 \rho_v d_i \left[\frac{\sigma(\rho_l - \rho_v)g}{\rho_v^2} \right]^{\frac{1}{4}} \tag{4.11}$$

For the current experimental condition, this correlation gives a critical heat flux of 161.23 kW/m². However, the experiment data showed in Fig. 10 are one order of magnitude less than this value.

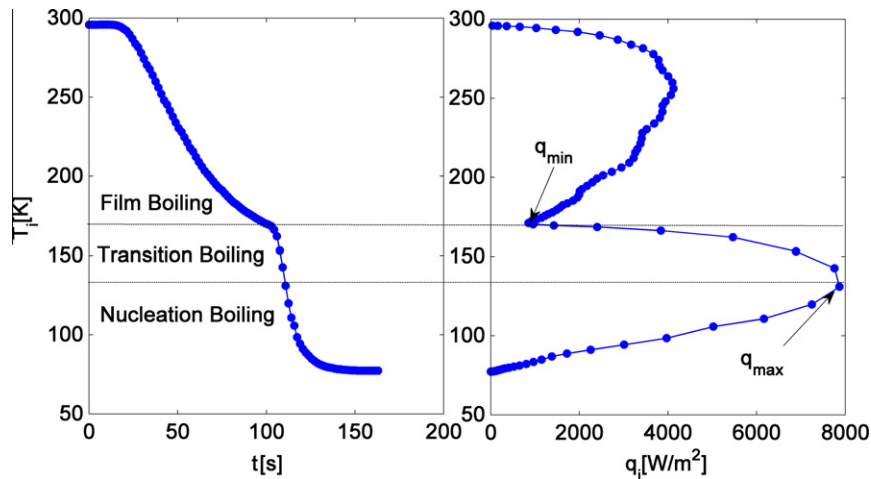


Fig. 7. Typical temperature and heat flux profiles in upward flow for $G = 66 \text{ kg/m}^2 \text{ s}$.

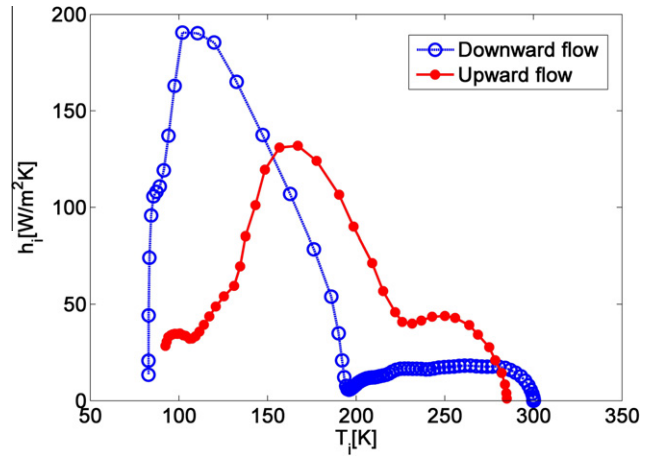


Fig. 8. Comparison of heat transfer coefficient profile between the upward and downward flows for $G = 66 \text{ kg/m}^2 \text{ s}$.

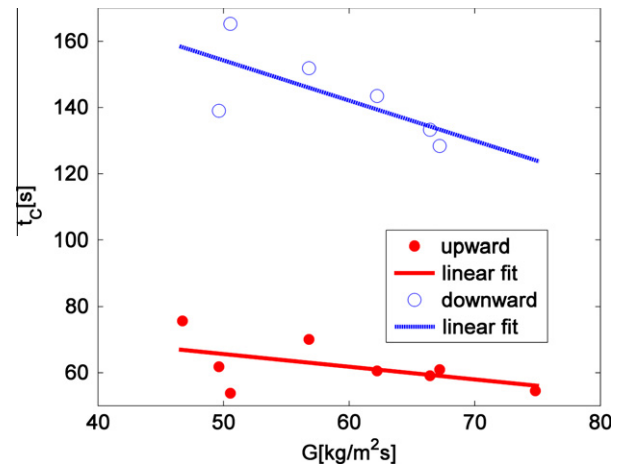


Fig. 9. Variation of the total chilldown time with mass flow rate.

The reason for these large differences partially comes from the different boiling mechanisms between chilldown and pool boiling. For the pool boiling, the heater is maintained either at constant temperature or constant heat flux. However, for the chilldown test, the energy for boiling is provided by the thermal energy, which is initially stored in the wall of the tube. This means that the heat flux and wall

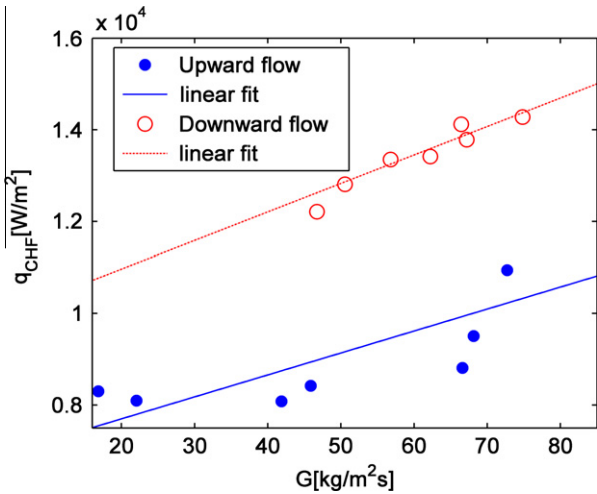


Fig. 10. Variation of the critical heat flux with mass flow rate.

superheat decrease continuously, which causes the driving force for boiling to become weaker. Moreover, the boiling correlation should have some kind of a relationship with the tube physical property. Actually, Zuber’s model is only concerned with the properties of the fluid, which also leads to differences. As Zhang et al. [21] stated that the CHF is very sensitive to the orientation for low mass flow rates. They came to the same conclusion that CHF data for the low velocity condition are under predicted by the Zuber’s model.

If compared to the data reported by Yuan et al. [16] on horizontal pipe chilldown experiments, current data is 60% less. One of the probable reasons for this is due to the gravity effect to a great extent. In their horizontal experiments, the gravity leads to the vapor–liquid separation, the liquid flowing at the bottom while the vapor on the upper part. Similarly, the gravity acted as a force normal to the bottom wall pushing the liquid to the bottom directly. However, in the current experiments, the lack of such a force results to local dry out easily and furthermore lower heat transfer coefficient.

From the above figures, one common finding is that the plot for the downward and upward flow are approaching to each other,

which means the effect of gravity is decreasing when mass flow rate is increasing. The reason for this can probably be explained as following. For the upward flow, the flow is decelerated but accelerated for the downward flow because of the gravity. Therefore the critical heat flux and heat transfer coefficient are larger for the downward flow than those for the upward flow because of the higher speeds. However, this difference on flow speeds between the upward and downward flows will decrease when the mass flow rate increases. The reason for this is that both acceleration and deceleration caused by gravity will affect less portion of the flow velocity. Therefore, it is expected that the flow will maintain a more constant velocity along the whole tube when mass flow rate increases. In another words, it can be predicted that the effect of mass flow rate will gradually overcome those of flow direction and gravity effect, when mass flow rate is high enough. Meanwhile, the chilldown time will be the same for both upward and downward flows.

4.2. Flow pattern development

From the previous analysis, it is clear that the chilldown process involves dramatic flow pattern development, which will further affect the heat transfer mechanisms. In order to investigate the special distribution of vapor and liquid varies varying with time, high speed camera was used to capture the flow pattern. The photographs will provide insight on how the flow pattern develops and its effect on heat transfer.

Fig. 11 provides a brief comparison on flow patterns between low and high mass flow rate conditions. The figure shows a fully developed vertical flow pattern typically for a cryogenic liquid, which assumes that the tube is long enough to show the complete flow pattern evolution from beginning to the end. Under a high mass flow rate, as shown in the middle images, two different flow patterns, inverted annular flow and bubbly flow have been observed during the chilldown tests. This sequence of flow patterns was observed by Kawaji et al. [22]. Inverted annular flow occurs at the beginning of the chilldown test when the wall temperature is higher than the rewetting temperature. Bubbly flow will be seen when the wall is cooled down to rewetting temperature and the liquid has a direct contact with the wall, which leads to the bubble nucleation. On the other hand, Kawaji et al. [22] have also recorded

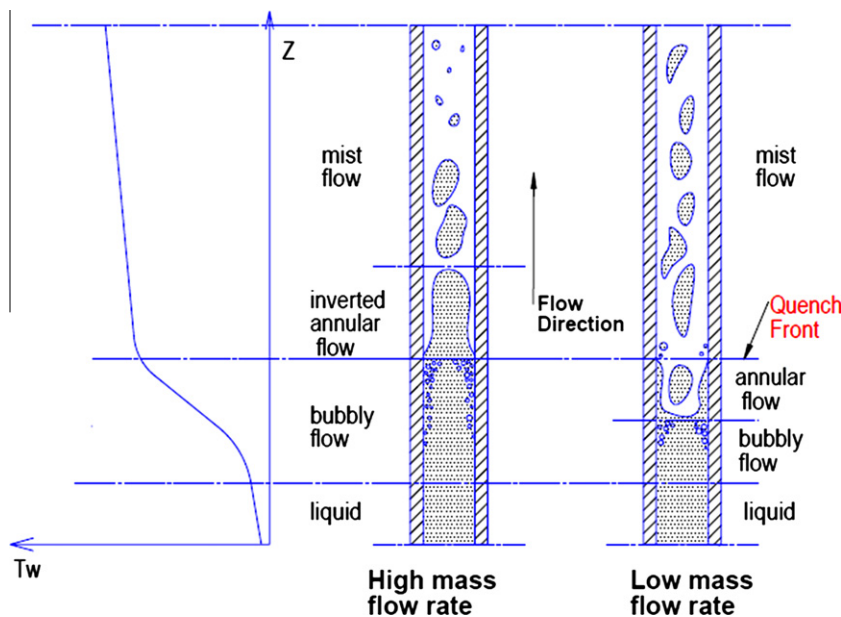


Fig. 11. Heat transfer regimes and flow patterns during quenching in a vertical pipe.

flow patterns for saturated flow at low mass flow rate, as the right images shows.

A series of photographs of flow pattern development is shown in Fig. 12. Under the present experimental condition, as the first pure gas will fill the whole tube because liquid is all turned to vapor in a short distance. Then, a dispersed flow comprised of small and spherical liquid drops embedded in the vapor is observed. With a further wall temperature decrease, the small droplets become dense and coalesce to form some larger and stretched droplets. After that, a continuous liquid core occurs which flows in the center of the tube and is surrounded by a thin layer of vapor film. This phenomenon is called the inverted annular flow. At this time, the film is thick enough to isolate the wall and liquid core efficiently. With a further decrease of the wall temperature, the vapor film becomes thinner while the liquid core will occupy more area. When the wall temperature is reduced to the rewetting temperature, the liquid is able to come into a direct contact with the channel walls. Some short liquid filaments can be seen. The transient boiling, characterized by intermittent liquid-wall contact and violent bubble generation, is observed during a limited period. The vapor–liquid interface is highly wavy because of Kelvin–Helmholtz instability. Quenching front will occur when the wall temperature reaches the CHF corresponding temperature. At this time the heat transfer rate from the hot wall to the liquid is significantly increased and a rapid drop of the wall temperature slope can be observed. A rapid change from the transition flow to the dispersed

bubbly flow will occur directly after the quenching front. The prevailing boiling regime is the nucleate boiling with clear small bubbles generated at the wall.

According to Carey [17], the stability of a vapor–liquid interface depends on the relative velocity between the two phases and is also linked to the gravity acceleration and the fluid physical properties such as the surface tension and density difference between vapor and liquid phases. Therefore, when the liquid velocity is limited but the vapor velocity is high, the interface is quite unstable and the liquid core is irregular during the quench phenomenon. On the contrary, when the liquid flow rate is high enough, and the relative velocity between the two phases decreases, the interface is stable and the liquid core is characterized by a regular and smooth shape.

Based on the vertical quenching tests performed both on earth and in a parabolic flight using FC-72, Celata et al. [14] have come across a similar conclusion that for low mass flow rates, the liquid core is irregular, and continuously formed and disrupted during the cooling process, while for higher mass flow rates the liquid core is more stable and regular.

4.3. Quenching front characteristics

Quenching front behavior is also a topic of this research, because quenching front is concerned with the critical heat flux and therefore the total time required for chilldown. Some

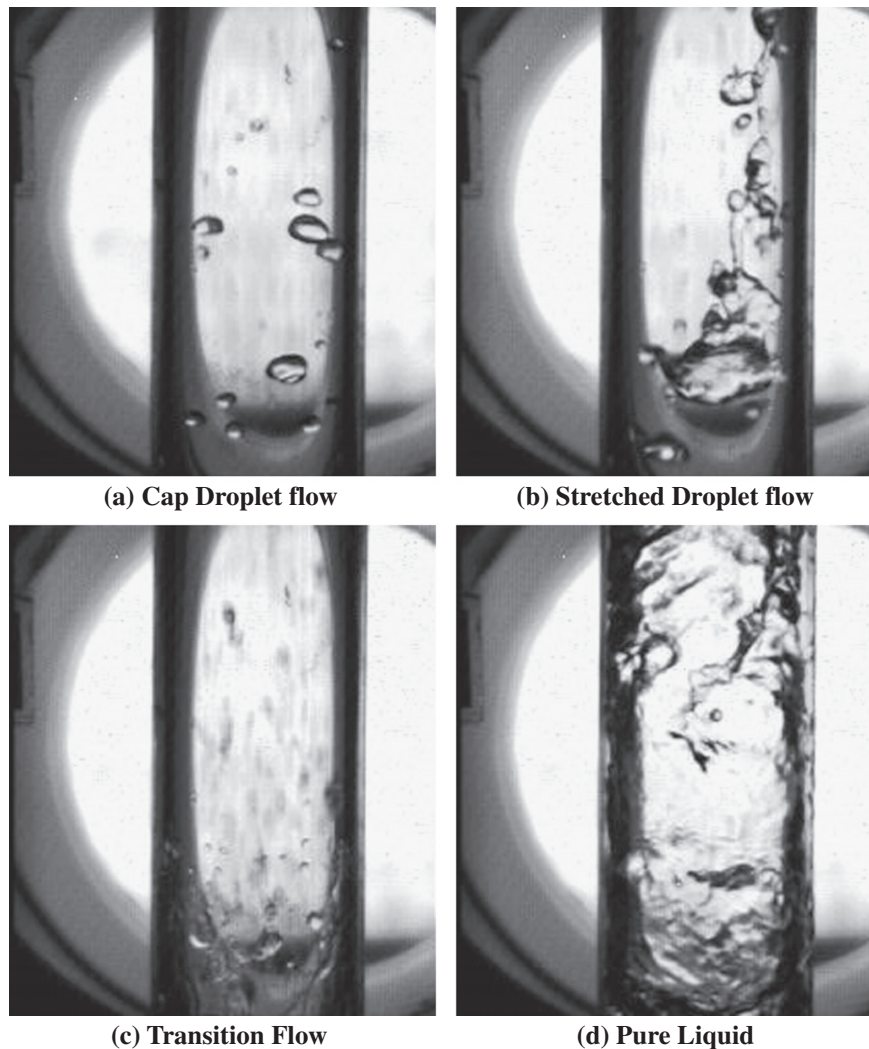


Fig. 12. Flow pattern development for upward flow $G = 45 \text{ kg/m}^2 \text{ s}$, $T_w = 290 \text{ K}$.

researchers [25] believed that quenching front has some kinds of relationship with the mass flow rate and tube diameter. This study will connect the quench front movement with mass flow rate and flow orientations.

There have been a lot of different ways used to define the quenching front by different researchers. Westbye et al. [12], Celata et al. [14] and Chen et al. [23] prefer to use the rewetting temperature T_{rew} to define the apparent rewetting temperature obtained by drawing the tangents on the transient temperature curves in the regions where a significant change of the curve slope occurs, as schematically drawn in Fig. 13. T_{rew} marks the onset of a rapid surface cooling caused by an enhanced rate of heat transfer that does require a liquid–solid contact. Some researchers [10] have pointed out that the rewetting temperature is the one at which a triple-phase, vapor–liquid–solid contact line is formed. The extreme portion of the surface rewetted by the coolant is called quench front. The quenching front velocity indicates the speed at which the quench front moves from the inlet along the hot tube, and is responsible for the time required for the rewetting of the whole tube. For the current experiment, the tangent on the transient temperature curves is used to define the quench front.

Although, it is difficult to get clear photographs for cryogenic flows due to its fast speeds and the moisture caused by a strong boiling in the liquid nitrogen, the movement of the quench front obtained through a high speed camera is shown in Fig 13, in which red lines are used to highlight the quench front.

The quenching front in a vertical pipeline should be nearly proportional to the wall surface condition, which is very similar to that in the microgravity condition. However, the interface instability will cause waves for the quench front formation at low mass flow rates in the current experiment.

The rewetting temperature is observed to increase with increasing mass flow rate under both conditions. From Fig. 14, it is also apparent that rewetting temperature increases more rapidly with the mass flow rate in a downward flow as compared to an upward flow. According to Chan's model [24] and Westbye's analysis [12]

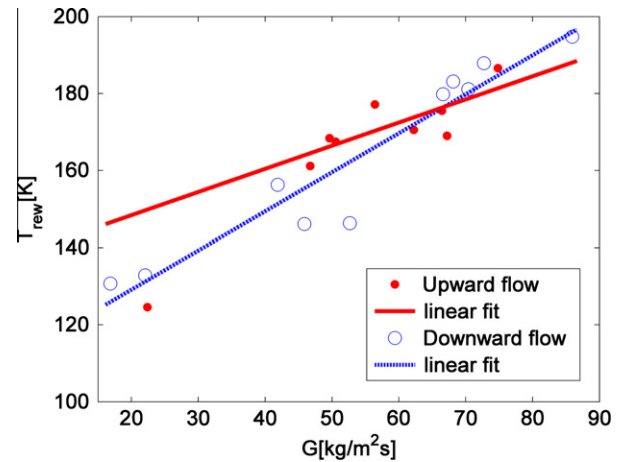


Fig. 14. Variation of the rewetting temperature with mass flow rate.

on a horizontal pipe, rewetting temperature has a close relationship with the Kelvin–Helmholtz type instability. When the vapor film thickness increases, the rewetting temperature will decrease. This explains the reason for a reduction in rewetting temperature in a relatively low mass flow rate region for the downward flow. However, when the mass flow rate is high enough, the film thickness is determined by the mass flow rate to a larger extent. A larger mass flow rate will press the film thinner and closer to the wall. For the downward flow, the flow velocity is relatively higher due to gravity. Therefore, it is reasonable that the rewetting temperature is higher for downward flow than that for the upward flow in a large mass flow rate.

Quenching front velocity is related with many factors including mass flow rate and wall superheat. Some researchers [25] have pointed out that the heat transfer coefficient increases with sub-cooling which can partially explain the higher quenching front

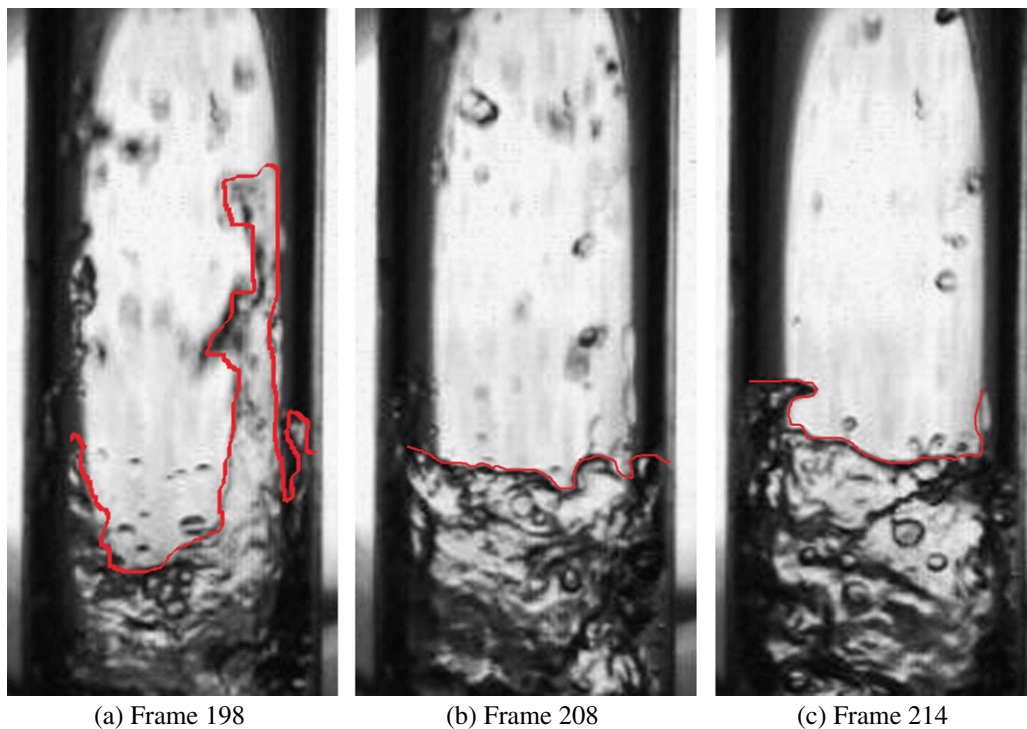


Fig. 13. Three single frames showing quench front movement of upward flow, $G = 45 \text{ kg/m}^2 \text{ s}$.

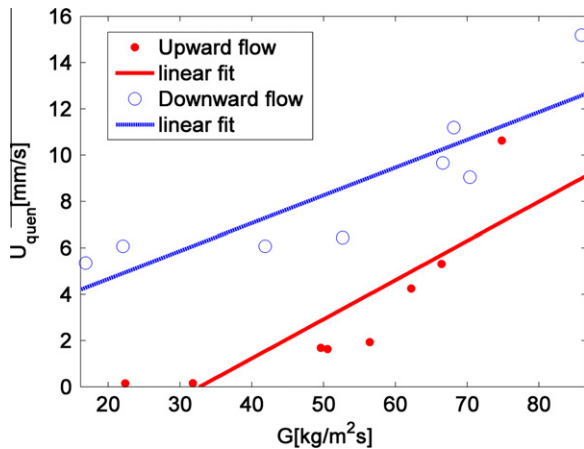


Fig. 15. Variation of the quenching front velocity with mass flow rate.

velocities measured for higher flow rates and inlet sub-cooling. For the current test, the inlet fluid is maintained at the saturated temperature. Therefore, mass flow rate will become the main factor. Adham-Khodaparast et al. [26] have come to the similar conclusion on rewetting temperature using R-113. Celata et al. [14] have concluded that the quench front is strongly affected by the mass flow rate and quench front velocity is always greater in downward flow than the corresponding upward flow. Based on the explanation given by Westbye et al. [12], it is reasonable to state that under the downward flow, the pipe is chilled down significantly before the quench front appears. According to Fig. 15, once the quench front occurs, it can propagate quickly because the wall temperature is low enough to establish a liquid-wall contact immediately.

5. Conclusion

In this paper, heat transfer during a vertical pipe chilldown process is studied. The test tube is made of Pyrex with inner diameter of 8.0 mm. Measurements including temperatures changes along the pipe corresponding to different mass flow rates were acquired through experiments using liquid nitrogen as the working fluids under terrestrial conditions. The results showed that both mass flow rate and flow direction affected the heat transfer characteristics.

- (1) Mass flow rate has a large effect on the rewetting temperature, critical heat flux and quench front movement. Rewetting temperature and quench front velocity increase with increasing mass flow rate, while the critical heat flux decreases.
- (2) Total chilldown time for the upward flow is longer than the downward flow. The critical heat flux and heat transfer coefficient are larger for the downward flow than for the upward flow. However, quench front movement velocity is smaller for the upward flow. Rewetting temperature does not show a clear relationship with the flow direction.

The mass flow rate has a far larger influence than the orientation in terrestrial gravity under a high mass flow rate and the orientation

only has some effects when the mass flow rate is low. However, there are still remaining questions regarding the effect of gravity. The following work will be the investigation on the thermal performance of the cryogenics during a chilldown process in microgravity condition in order to reveal more on the gravity effect.

References

- [1] NASA.org. Washington, DC: About the Space Launch System & Multi-Purpose Crew Vehicle. <http://www.nasa.gov/exploration/new_space_enterprise/sls_mpcv/index.html> [updated 08.12.11; cited 20.12.11].
- [2] Evans L. The large hadron collider. *Annu Rev Nucl Part Sci* 2011;61:435–66.
- [3] ten Kate HHJ. The ATLAS superconducting magnet system at the Large Hadron Collider. *Phys C: Supercond* 2008;468:2137–42.
- [4] Manera A, Prasser HM, Lucas D, van der Hagen THJJ. Three-dimensional flow pattern visualization and bubble size distributions in stationary and transient upward flashing flow. *Int J Multiphase Flow* 2006;32:996–1016.
- [5] Estrada-Perez CE, Hassan YA. PTV experiments of subcooled boiling flow through a vertical rectangular channel. *Int J Multiphase Flow* 2010;36:691–706.
- [6] Zhang P, Fu X. Two-phase flow characteristics of liquid nitrogen in vertically upward 0.5 and 1.0 mm micro-tubes: visualization studies. *Cryogenics* 2009;49:565–75.
- [7] Fu X, Zhang P, Hu H, Huang CJ, Huang Y, Wang RZ. 3D visualization of two-phase flow in the micro-tube by a simple but effective method. *J Micromech Microeng* 2009;19:085005–16.
- [8] Fu X, Zhang P, Huang CJ, Wang RZ. Bubble growth, departure and the following flow pattern evolution during flow boiling in a mini-tube. *Int J Heat Mass Transfer* 2010;53:4819–31.
- [9] Barnea Y, Ellas E, Shai I. Flow and heat transfer regimes during quenching of hot surface. *Int J Heat Mass Transfer* 1994;37:1441–53.
- [10] Antar BN, Collins FG. Flow boiling in low gravity environment. *Microgravity Sci Technol* 1997;10:118–28.
- [11] Kawanami O, Nishida T, Honda I, Kawashima Y, Ohta H. Flow and heat transfer on cryogenic flow boiling during tube quenching under upward and downward flow. In: 2nd International topical team workshop on two-phase system for ground and space applications, Kyoto, Japan; 26–28 October 2007.
- [12] Westbye CJ, Kawaji M, Antar BN. Boiling heat transfer in the quenching of a hot tube under microgravity. *J Thermophys Heat Transfer* 1995;9:302–7.
- [13] Verthier B, Celata GP, Zummo G, Colin C, Follet J. Effect of gravity on film boiling heat transfer and rewetting temperature during quenching. *Microgravity Sci Technol* 2009;21:185–91.
- [14] Celata GP, Cumo M, Gervasi M, Zummo G. Quenching experiments inside 6.0 mm tube at reduced gravity. *Int J Heat and Mass Transfer* 2009;52:2807–14.
- [15] Kawanami O, Azuma H, Ohta H. Effect of gravity on cryogenic boiling heat transfer during tube quenching. *Int J Heat Mass Transfer* 2007;50:3490–7.
- [16] Yuan K, Ji Y, Chung JN, Shyy W. Cryogenic boiling and two-phase flow during pipe chilldown in earth and reduced gravity. *J Low Temp Phys* 2008;150:101–22.
- [17] Carey VP. *Liquid vapor phase change phenomena*. New York: Taylor & Francis; 1992.
- [18] Ozisik MN. *Heat conduction*. 2nd ed. New York: John Wiley and Sons; 1993.
- [19] Ozisik MN, Orlande HRB. *Inverse heat transfer*. New York: Taylor and Francis; 2000.
- [20] Burggraf OR. An exact solution of inverse problem in heat condition theory and application. *J Heat Transfer* 1964;86:373–82.
- [21] Zhang H, Mudawar I, Hasan MM. Experimental assessment of the effects of body force, surface tension force, and inertia on flow boiling CHF. *Int J Heat Mass Transfer* 2002;45:4079–95.
- [22] Kawaji M, Ng YS, Banerjee S, Yadigaroglu G. Reflooding with steady and oscillatory injection: Part I—flow regimes, void fraction, and heat transfer. *J Heat Transfer* 1985;107:670–9.
- [23] Chen WJ, Lee Y, Groeneveld DC. Measurement of boiling curves during rewetting of a hot circular duct. *Int J Heat Mass Transfer* 1979;22:973–6.
- [24] Chan AMC, Banerjee S. Refilling and rewetting of a hot horizontal tube: Part I experiments. *J Heat Transfer* 1981;103:281–7.
- [25] Chambri P, Elias E. Boiling heat transfer during rewetting. *Nucl Eng Des* 1978;50:353–63.
- [26] Adham-Khodaparast K, Xu JJ, Kawaji M. Flow film boiling collapse and surface rewetting in normal and reduced gravity conditions. *Int J Heat Mass Transfer* 1995;38:2749–60.